UNSTEADY AERODYNAMIC PHENOMENA ON NOVEL WING PLANFORMS

M.I. Woods and N.J. Wood
School of Mechanical Engineering
University of Bath, UK.

Abstract

The results of wind tunnel tests carried out on a series of generic 40° leading edge sweep semi-span models are presented. The planforms investigated have been specified as having features likely to be encountered on future low observable aircraft and were constructed utilising a foam/composite construction technique. Dynamic calibration of surface pressure tappings has allowed both time-averaged and unsteady pressures to be measured over the entire upper surface of each wing. In addition, balance and buffeting data has been acquired to angles of attack beyond stall. Unsteady pressure time histories have been spectrally analysed for dominant frequencies and their magnitudes.

Maximum RMS pressures are observed in the primary attachment region of the leading edge vortex system. The dominant buffet frequency is shown to be dependant on the chordwise location, incidence and free stream velocity as expected. A second buffet frequency, of equal significance and twice the frequency, has been identified in the region of vortex attachment.

Nomenclature

$\bar{\bar{c}}$	mean aerodynamic chord
C_p	pressure coefficient
f	frequency
n_m	modified reduced frequency parameter
$\bar{p}$	RMS pressure
p(f)	pressure output by speaker
q	free stream dynamic pressure
r(f)	response function of tubing
s	wing semi-span
S	wing area of model
U_∞	freestream velocity
x	chordwise distance from apex
y	spanwise distance from root
α	incidence
ρ	air density

Abbreviations

FFT	Fast Fourier Transform
PSD	Power Spectral Density
RMS	Root Mean Square

Introduction

The configuration of a modern military aircraft is increasingly determined by constraints other than aerodynamic performance. Of increasing importance is the radar cross section (RCS) of the aircraft. The compromise between aerodynamics and these other emerging technologies has resulted in the generation of wing planforms (e.g. B-2, F-117) which are novel compared to existing aircraft and are unfamiliar to aerodynamicists.

Simultaneously, changes in air combat tactics are occurring with the development of aircraft systems technologies, new air to air weapons and advanced control systems[1]. Studies of modern combat scenarios[2] have shown that the ability to change attitude rapidly in order to out-manoeuvre an adversary to obtain the first firing opportunity provides a significant tactical advantage.

At angles of attack appropriate for a manoeuvring combat aircraft it is possible that large amounts of flow induced excitation (buffet) would be encountered. Should the frequency distribution of the buffet overlap one or more structural modes then significant response of the structure (buffeting) may result. This is clearly undesirable and may result in a reduction of the flight envelope and/or in-service repair or replacement modifications. In addition, the external profile of a modern combat aircraft is less likely to be modified (at any point in the design process) to enable suppression of excessive buffet since these aircraft will be less amenable to conventional 'fixes' such as strakes and vortex generators due to the RCS penalty of such devices. As a consequence, modifications to accommodate additional dynamic loads result in significant increases in internal structure weight and complexity. It is therefore desirable to be able to predict the buffet loads such that they can be minimised during the early design stage of an aircraft and then accounted for from both strength and fatigue viewpoints during the detailed design process.

The presence of discontinuities in the leading and trailing edges of future generation wings, together with the sharp peripheries required for low observability characteristics, lead to the production of strong coherent vortices which have recently been shown to exhibit

distinct characteristic frequencies of excitation[3,4,5,6] particularly when a vortex burst is present over the wing upper surface. A modified reduced frequency parameter has been proposed[7] of the form:

$$n_m = \frac{f\bar{c} \sin \alpha}{U}$$

This parameter has origins from investigations on the phenomenon of fin buffeting and represents the centre frequency of the buffet at the trailing edge of a delta wing. It has been shown that the parameter is dependant on sweep angle and there is some evidence to suggest a simple relationship between the centre frequency and chordwise location on the wing[8]. An alternative view is to consider that n_m represents a relationship between a particular wing planform and the movement of the vortex burst over the wing with increasing angle of attack.

In order to establish a design procedure it is necessary to know the spatial distribution of the buffet and the dominant frequencies it contains for an arbitrary wing planform. Thus it is important to relate the unsteady excitation to the mean flow topology which it is assumed can be approximated with increasing accuracy by modern numerical methods. Subsequently a combination of steady flow computation to predict the mean flow and empirical prediction of frequency and amplitude could be used to generate load time histories for detailed structural design early in the design cycle.

The objective of the present research was therefore to investigate the effects of wing planform on the buffet excitation and in particular to consider the development of non-dimensional frequency and amplitude parameters which account for planform variations.

Experimental Details

A series of wind tunnel models were fabricated for testing in the University of Bath low speed wind tunnel. Novel manufacturing techniques were used to expedite model production. The successful development of dynamic calibration of steady surface pressure measurement systems enabled extensive coverage of the wings upper surface to reveal previously unseen detail within the buffet distribution. This could be coupled with more conventional techniques for buffeting measurement, flow visualisation and balance measurements to provide a comrehensive suite of experimental data.

Model Construction

Two semi span models were constructed with planforms as shown in figure 1, the leading and trailing edge sweep angle of each model was 40°. The models will be referred to as rhomboid and lambda respectively. Each wing was constructed from a foam core which was hand finished between templates and an outer 'cloth' skin of either glass or carbon fibre. The outer skin was secured using cold cured epoxy resin and multiple layers could be used to increase the model stiffness as required. This technique produced lightweight models of high stiffness which resulted in relatively high wing first bending structural modes thus avoiding problems of resonance. Within the entire programme, two further models were produced and represented a 40° sweep baseline wing with no trailing edge sweep and a 'Y' wing similar to the lambda wing but with a sweep angle of 60°. In the interest of brevity, results from those models will not be presented in this paper.

To simplicify manufacture, the upper surface of each model was flat, and tappings were formed on this surface by laying VINL-063 Scanivalve® tubes into the Styrofoam IB core of the wing, bonding a glass fibre skin to the surface and drilling a perpendicular hole directly into the vinyl tube. A carbon fibre skin was bonded to the convex lower surface of each model. In addition to the surface pressure tappings, each model was equipped with 6 Entran EPE-701-2P pressure transducers which were co-located with surface pressure tappings and up to 6 Entran EGA-125F-25D miniature accelerometers to monitor the buffeting response. Each model took typically two man months to fabricate from start to tunnel entry. Surface dimensional accuracy was better than 1mm which for the separated flow of interest was acceptable. Sharp edges were maintained by hand finishing each model. All wind tunnel models exhibited first bending frequencies in the range of 35 to 70Hz and were statically tested to twice maximum expected load prior to tunnel entry.

Instrumentation and Data Analysis

Signals from the accelerometers, unsteady pressure transducers, transducers contained within the Scanivalve system and six component balance were monitored and controlled by a Personal Computer (PC) based acquisition system utilising the software DT-Vee™ by Data Translation®. The system used is shown schematically in figure 2. The Analogue to Digital (A/D) and Digital to Analogue (D/A) subsystem was a DT2839 data acquisition board by Data Translation®. This board was connected to the sensors via standard in-house fixed gain DC amplifier cards.

The system for converting unsteady pressure data to PSDs is shown schematically in figure 3. Static pressure calibrations were applied and FFTs calculated within the DT-Vee™ by software and sent to Microsoft Excel by a Dynamic Data Exchange (DDE) link. Unsteady pressure calibrations were then applied and PSDs calculated within Microsoft Excel. The PSDs were non-dimensionalised with the square of the free stream dynamic pressure and the RMS buffet was obtained after calculating the area beneath the PSD curve from 10 to 500Hz[9].

Surface Tapping Dynamic Calibration

To allow unsteady pressure to be measured over the entire upper surface of the wing, the response function r(f) of the surface pressure tubing system connecting the tapping to the pressure transducer within the Scanivalve® unit was required. The calibration system is shown schematically in figure 4. A PC controlled loudspeaker was used to generate a calibration signal which was configured such that the amplitude of pressure oscillation output by the speaker p(f) was constant between 8 and 500Hz. Hence the complex Fourier Transforms of the pressures measured at the wing surface and the Scanivalve unit are p(f) and p*r respectively. Therefore r(f) can be calculated simply by dividing p*r by p(f). Variations in the internal dimensions of the tubes and surface imperfections on the wing necessitated that each tapping was calibrated individually. An example of a typical response function is shown in figure 5. The shorter tube calibration shows evidence of a resonance around 200Hz but this does not affect the data quality. Longer tubes exhibit resonance at lower frequencies but with higher damping. To validate the data quality, the PSDs at six of the pressure tappings were compared with those of co-located pressure transducers. An example of such a comparison is shown in figure 6. The narrow spike near 35Hz is the wind tunnel fan blade passage frequency and is therefore a function of tunnel free stream speed. Since this is known it is simply removed from the subsequent data analysis and does not contribute to the RMS calculations. The main development within the present research was the extension of the method to include frequencies up to 500Hz. This limit was imposed since the flows of interest were expected to exhibit centre frequencies of less than 100Hz. It is worth noting that this is near the upper limit of the recommended operating range of most miniature pressure transducers.

Wind Tunnel Testing

The semi span models were tested in the 2.13x1.52m low speed wind tunnel at the University of Bath as shown in Figures 7 and 8. Model incidence could be adjusted in the range ±90° although a typical operating range was from -5° to +30°. Results are presented for tunnel speeds of between 20 and 30m/s, resulting in Reynolds Numbers of between 1.35×10^6 and 2.0×10^6 per metre. Force and moment data was acquired using the six component balance installed above the tunnel test section.

Experimental accuracy and repeatability

The stochastic nature of buffet and buffeting signals is well known[10] and makes the determination of the optimum data acquisition parameters, such as sample rate and time, of paramount importance to ensure the reliability and repeatability of results without being wasteful in terms of tunnel and analysis time.

Both buffet and buffeting repeatability were assessed. This was achieved by completing 20 identical tunnel runs at $30ms^{-1}$ and acquiring both buffet and buffeting data for 60 seconds. The spread of the RMS of the signals was then considered against sample time. An example of this is shown in figure 9. It is clear from this result that the percentage spread in the RMS signals reduces at large acquisition times. These tests were repeated for each tunnel entry typically near peak buffeting to achieve consistent repeatability and reliability. Sample times of 30 seconds and 25 seconds were selected for buffeting and buffet data respectively. Standard deviations of RMS values were less than 1.5% for buffeting and 2.0% for buffet data throughout the incidence range. Sampling duration, rate and analysis parameters were set to maintain a 2Hz frequency resolution on all PSDs.

Results

Lift curves for both configurations are shown in figure 10, the low values of lift curve slope reflecting the low aspect ratio of the wings. Maximum lift is achieved at incidences of 20° and 22° for the rhomboid and lambda wings respectively. The positive zero lift angle of attack reflects the negative camber of each wing section formed by the flat upper surface and convex lower surface.

Buffeting profiles together with diagrams of accelerometer positions are shown in Figures 11 and 12. Those accelerometers shown at the wing roots are attached to the model support system and the low measured levels of buffeting confirm the other responses to be the result of buffet induced motion. Peaks in the profiles are apparent in the pre-stall region for all configurations with maximum buffeting taking place at incidences of 13° for rhomboid and at 14° for the lambda wing. Maximum RMS wingtip deflection (obtained

from integration of the buffeting response) was of the order of 0.2mm. Onset of buffeting takes place at incidences of 6° for rhomboid and at an incidence of 3° for the lambda wing. The absolute magnitudes of buffeting may not be compared since the structural modes of each wing are slightly different and the tests were run at a fixed tunnel speed.

Levels of RMS buffeting for the lambda wing reach a plateau between incidences of 6° and 9°. Oil flow visualisation for that planform at an incidence of 8° is shown in figure 13. The primary attachment of the leading edge vortex system is aligned with the 'reverse apex'; the reflex angle on the trailing edge of the planform. Consideration of flow visualisation at other angles of attack showed that the trajectory of the leading edge vortex attachment line appears to have been constrained by the discontinuity in the trailing edge. This is thought to generate the observed plateau in the buffeting profile. As the incidence is increased beyond 9° the primary attachment moves inboard of the reverse apex and the levels of RMS buffeting rise as expected. The dominant response is in the wing first bending mode.

Contour plots of the steady pressure coefficients over the upper surface of the rhomboid and lambda wings at incidences of 14° are depicted in Figures 14 and 15 (flow is from left to right). The small individual symbols on each plot indicate the surface pressure tapping locations. The distributions indicate the presence of a weak leading edge vortex system for each model which is consistent with the relatively low sweep angle and as expected, the minimum steady pressure coefficient is found under the core of the vortex.

The magnitude of the suction peak near the wing apex increases up to the stall angle of attack. The diffusion of vortex suction due to vortex burst[11] is difficult to detect due to the weak nature of the vortex, although a burst vortex is certainly present forward of the trailing edge for incidences higher than approximately 10° for each planform as verified by surface oil flow visualisation. At angles of attack beyond stall, the pressures still maintain a characteristic vortex signature but at significantly reduced suction levels.

Contours of RMS pressures are shown for the rhomboid and lambda wings on Figures 16 and 17 respectively. The steady pressure coefficient distribution is superimposed on the RMS amplitude along lines essentially normal to the vortex track in Figures 18a-b. It is clear that the peak RMS is associated with a location close to the attachment area of the vortex shear layer rather than the vortex core. There is some suggestion that the peak coincides with the inflexion point in the pressure distribution on the inboard side of the vortex. This result is of significance since many researchers place surface instrumentation to measure unsteady loads under the vortex core which is clearly not the most appropriate location.

The number of surface pressure tappings also enables interrogation of the PSDs at locations which include the peak rms, figure 19. For brevity, only data from the lambda wing will be displayed since all the features are also present on the rhomboid wing. A single low amplitude peak in excitation is apparent under the vortex core and a second, first harmonic, is present in the region of high rms. Inboard of that location the distribution returns to a single peak but at some intermediate frequency. This result is very significant. To the authors knowledge, the twin frequency result has not been previously measured. Prior to considering the variation of these frequencies it is worth examining their dependency on chordwise location.

Consideration of frequency domain information in the region of high RMS pressures, figure 20, indicates that both frequencies observed at points near the attachment region increase towards the wing apex.

The results from figures 19 and 20 may be summarised by consideration of the frequency parameter n_m along the attachment region of the vortex, figures 21 and 22. Previous work would suggest that a value of n_m of 0.3 would be appropriate for this sweep angle and it is clear that this is relevant to the frequency content under the vortex core. However, as shown on figures 19 and 20, a high proportion of the RMS near the attachment region is at a frequency which is represented by n_m of 0.6. The vast majority of research has only considered surface buffet in relation to the vortex core location and hence this additional frequency content has not previously been observed.

The mechanism for the lower frequency buffet has recently been shown to be related to the presence of a spiral type burst mechanism[12] which can be shown, by velocity correlation measurements, to exist to high Reynolds numbers. Thus the low frequency is related to a 'one per rev' passage of concentrated vorticity within the vortex shear layer. Presumably the impact of the shear layer at the attachment region and its subsequent translation across the surface to the leading edge gradually damps out the velocity fluctuations and this is reflected in the reducing amplitude in figures 18 and 19. The source of the higher frequency content is less clear since it has only recently been identified. Consideration could be given to a harmonic which is associated with the movement of the attachment line in much the same way as an impinging jet exhibits a natural frequency. In

this case the motion of the attachment line is related to the transit of the coherent packets of vorticity in the shear layer and hence the frequency doubling. At present no data can confirm this hypothesis since the phenomenon has only recently been observed. The third frequency detected inboard of the attachment region is also unusual and remains an area for further investigation.

These results are of great importance to research in wing buffet. Not only has it been shown that peak amplitudes (and hence improved signal to noise) are obtained by examination of buffet signals close to reattachment but there also exists a first harmonic excitation of high amplitude; this second frequency being restricted to this region. The implications for application within a preliminary design process are significant in that not only would current techniques underestimate the primary excitation amplitude but also they would ignore the presence of the higher harmonic.

Conclusions

The unsteady pressure measurement technique has allowed unsteady pressures at frequencies of up to 500Hz to be measured using a standard Scanivalve installation. The detailed coverage of the wing upper surface has enabled features of the separated flow to be observed in more detail than before at a significantly reduced cost compared to conventional techniques.

The novel planforms under consideration all have a weak leading edge vortex system present over the upper surface. Vortex burst, although difficult to track due to the weak nature of the vortex, is certainly present forward of the trailing edge of all the models at incidences greater than 10°. Onset of buffet for the model with a discontinuity on the trailing edge is rapid and takes place at an incidence of only 3°. This rapid rise in wingtip acceleration is followed by a plateau in the buffeting response between 6° and 9°. Between these angles of attack the primary attachment of the leading edge vortex is coincident with the 'reverse apex'.

Maximum RMS pressures are apparent in the primary attachment region of the leading edge vortex system rather than under the vortex core. Two distinct frequencies exist within the vortex attachment region the first at frequencies already measured near the track of the vortex core, the second at twice that frequency. Both frequencies adopt similar forms of the buffet frequency parameter which adequately describes the variation with angle of attack, free stream speed and chordwise location. The frequencies measured are consistent with a spiral type burst mechanism despite the relatively high Reynolds number.

Acknowledgements

This research was funded by Engineering & Physical Sciences Research Council Grant number GR/J86902 in collaboration with British Aerospace Defence (Military Aircraft Division), RD1 ref. no. WAP04GAAN, R & D Activity 2.3.A.3.

References

1) Lang J.D., Francis M.S., Unsteady Aerodynamics and Dynamic Aircraft Manoeuvrability, AGARD CP-386, April 1985
2) Herbst W.B., Dynamics of Air Combat, Journal of Aircraft, Vol. 20, No. 7, pp 594-598, July 1983
3) Bean D.E., The Analysis and Suppression of Vortex Induced Unsteady Loads at High Angles of Attack, PhD Thesis, School of Mechanical Engineering, University of Bath 1992.
4) Gordnier R.E., Visbal M.R., Unsteady Vortex Structure over a Delta Wing, J. Aircraft, Vol 31, No. 1, Jan-Feb 1994. pp243-248
5) Lowson M.V., The Three Dimensional Vortex Sheet Structure on Delta Wings, AGARD CP-438, Oct 1988. 11.1-11.16
6) Rediniotis, O.K., Stapountzis, H., Telionis, D.P., Periodic Shedding over Delta Wings. AIAA Journal Vol. 31, No. 9, September 1993. pp1555-1562
7) Mabey D.G., Measurements of Fin Buffeting on an 'F-18' Model and a Derived Interpretive Hypothesis, DRA Technical Memorandum AERO 2224, September 1991
8) Gursul I., Unsteady Flow Phenomena over Delta Wings at High Angle of Attack, AIAA Journal vol. 32, No. 2, February 1994. pp.225-231
9) Bendat J.S., Piersol A.G., Random Data: Analysis and Measurement Procedures, John Wiley and Sons, New York, 1971, ISBN 0-471-06470-X
10) Chesneau T.R., Wood N.J., Foreplane Effects in Single Fin Buffeting, International Forum on Aeroelasticity and Structural Dynamics, Manchester, UK, 1995, pp 51.1 -51.12
11) Greenwell, D.I., Wood, N.J., Determination of Vortex Burst Location on Delta Wings from Surface Pressure Measurements, AIAA Journal, Vol. 30, No. 11, November 1992, pp2736-2739
12) Jaworski, A.J., A Study of Pressure Fluctuations Caused by Vortex Breakdown, PhD Thesis, Imperial College, University of London, 1996

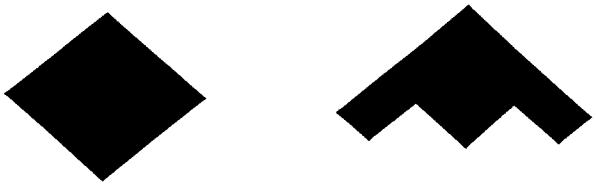

Model 2: Rhomboid

Model 3: 'Lambda'

Figure 1: Planforms Under Investigation

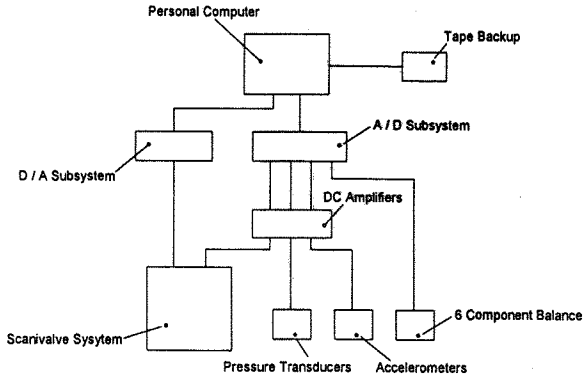

Figure 2: Data Acquisition System

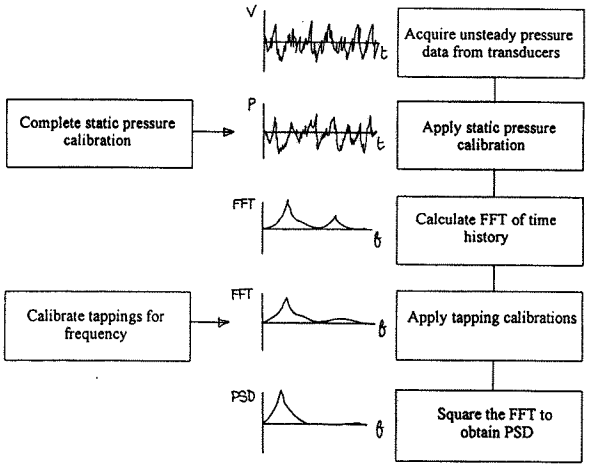

Figure 3: Unsteady Data Reduction

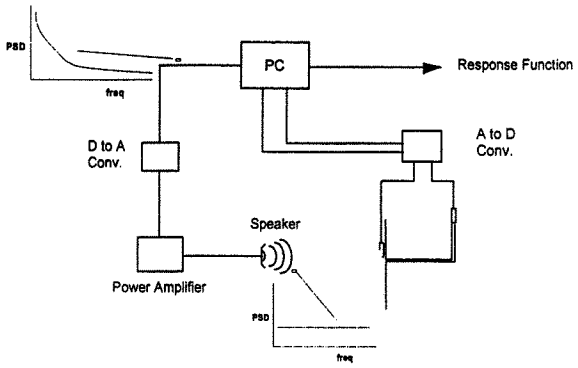

Figure 4:Tubing Calibration System

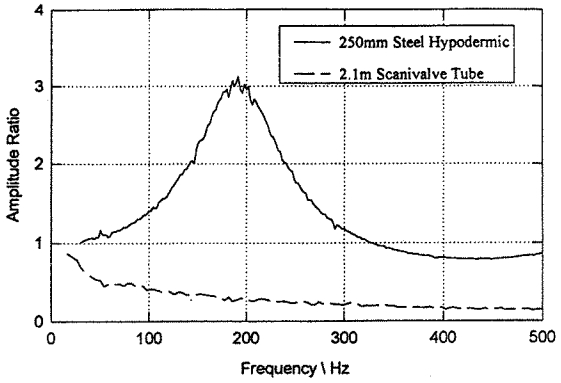

Figure 5: Typical Response Functions

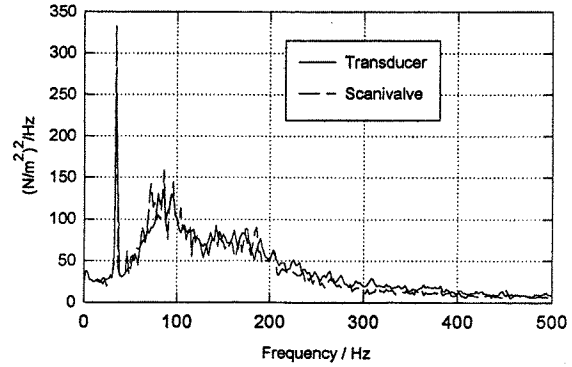

Figure 6: Transducer / Calibrated Scanivalve Comparison

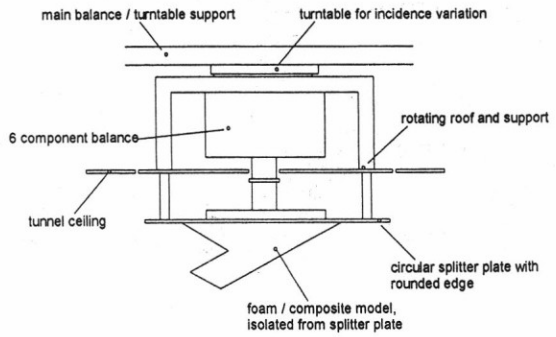

Figure 7: Wind Tunnel Installation

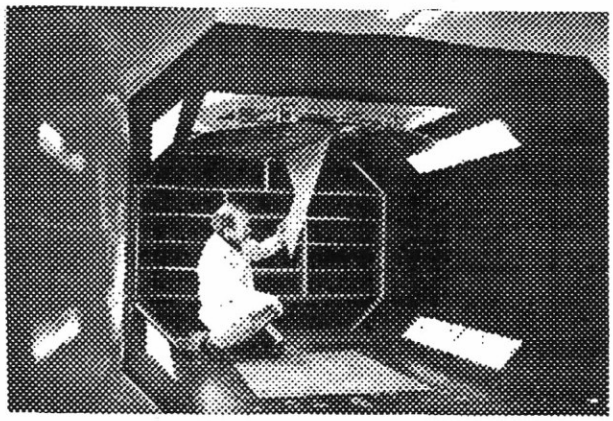

Figure 8: Model Installed in Wind Tunnel

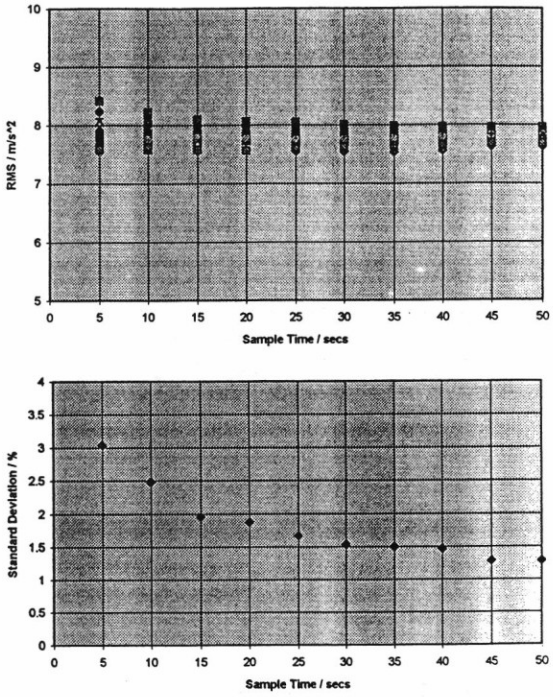

Figure 9: Data Quality Assessment

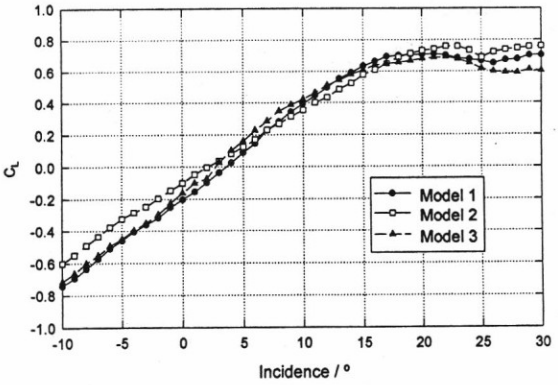

Figure 10: Lift Curves

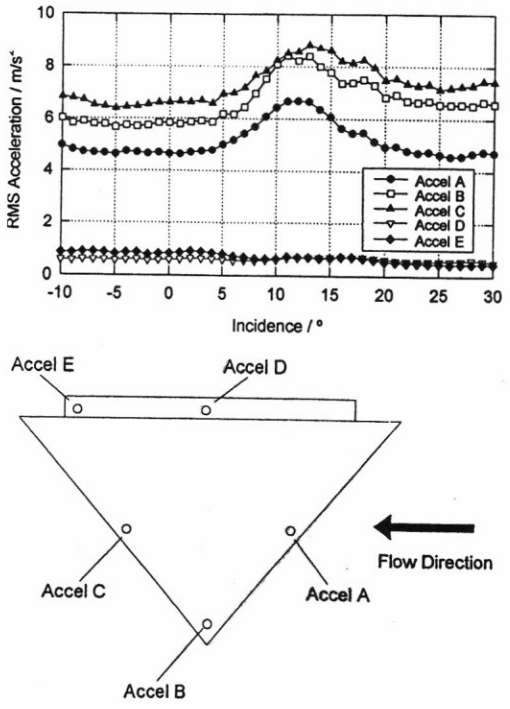

Figure 11: Model 2 Buffeting Profile

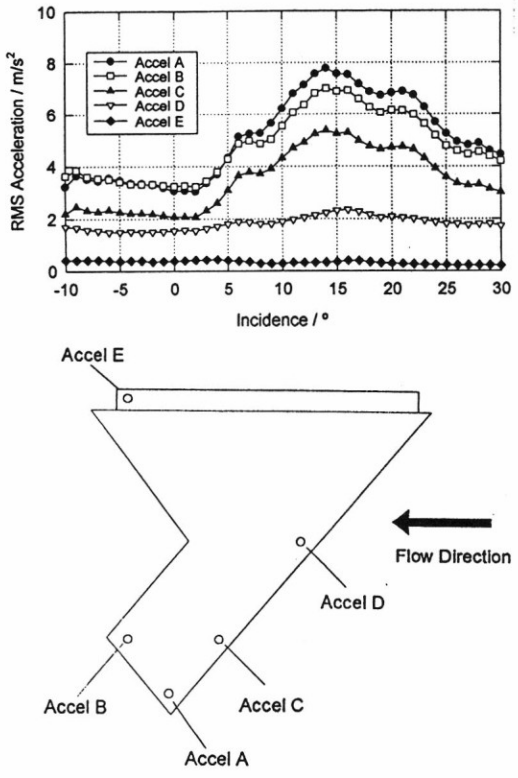

Figure 12: Model 3 Buffeting Profile

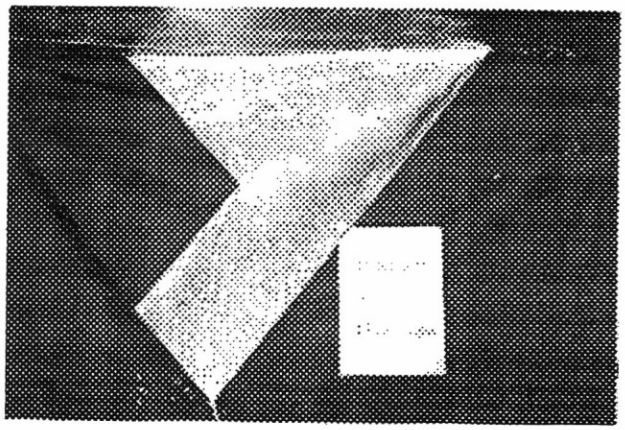

Figure 13: Surface Flow Visualisation, $\alpha = 8°$

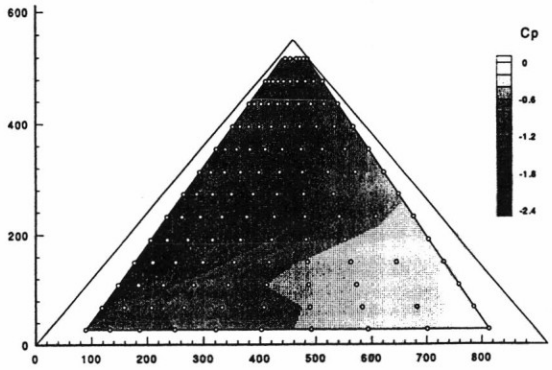

Figure 14: Model 2 Steady Pressures, a = 14°

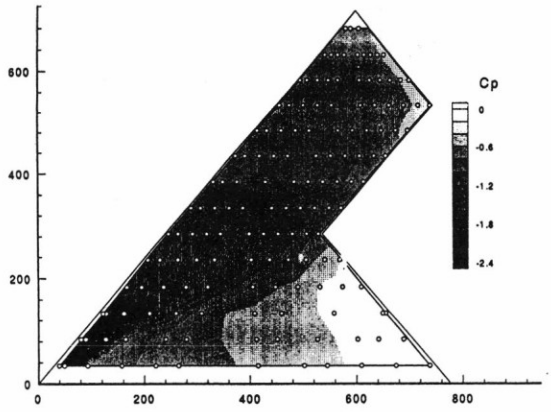

Figure 15: Model 3 Steady Pressures, $\alpha = 14°$

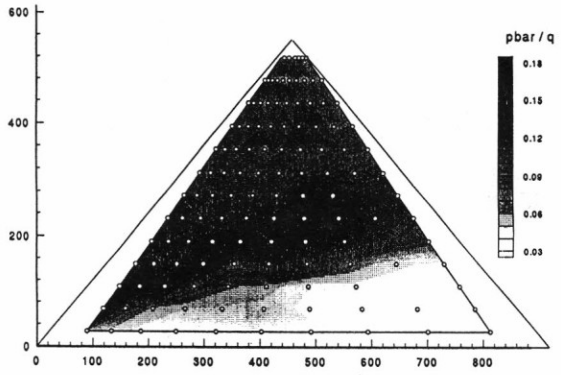

Figure 16: Model 2 RMS Pressures, $\alpha = 14°$

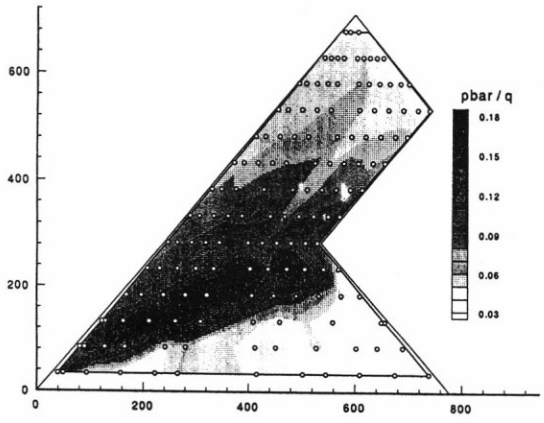

Figure 17: Model 3 RMS Pressures, $\alpha = 14°$

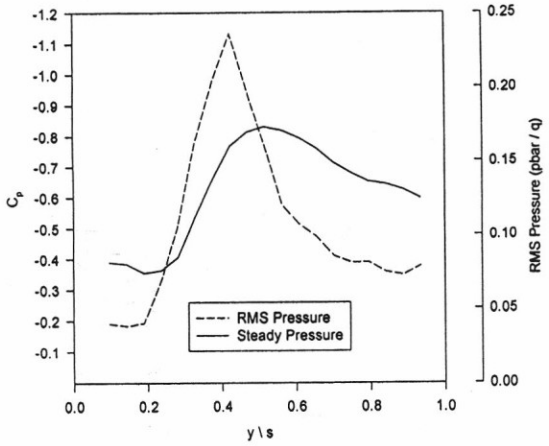

Figure 18a: Spanwise Variation of Steady and RMS Pressures - Model 2, $\alpha = 14°$

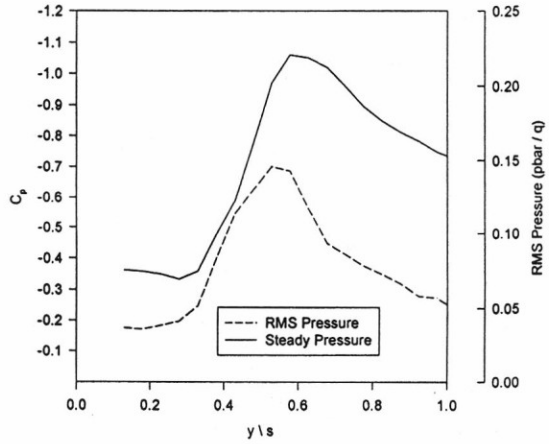

Figure 18b: Spanwise Variation of Steady and RMS Pressures - Model 3, $\alpha = 14°$

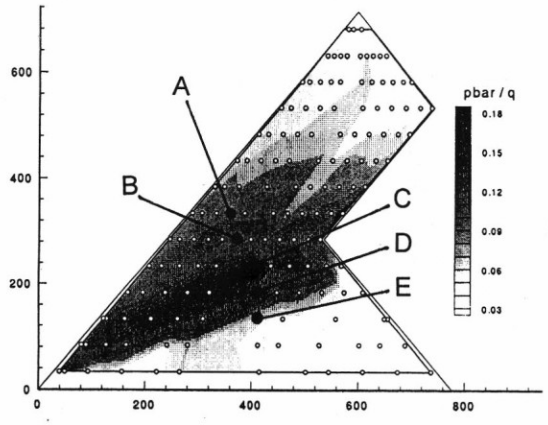

Figure 19a: Sample PSD Locations

PSD 'A'

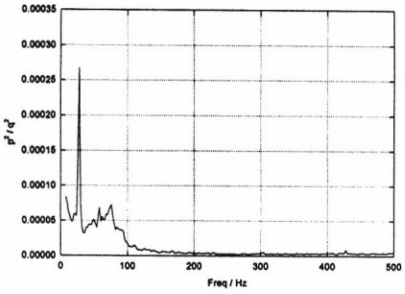

PSD 'B'

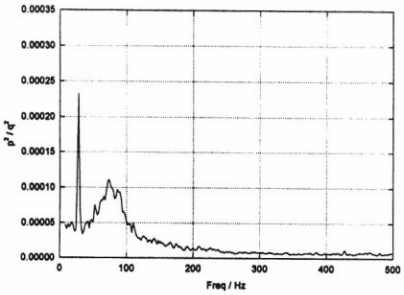

PSD 'C'

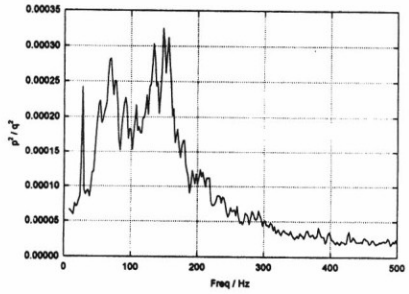

PSD 'D'

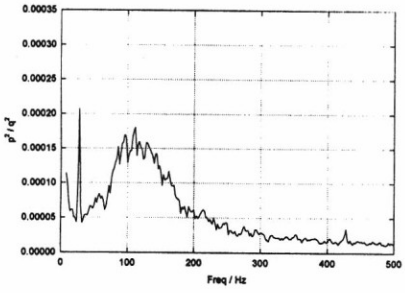

PSD 'E'

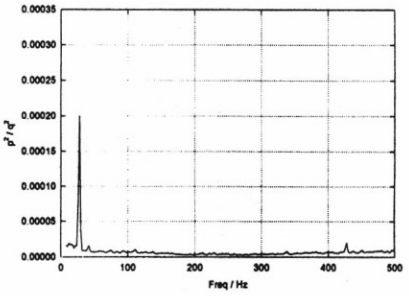

Figure 19b: PSDs Across Region of High RMS Pressure

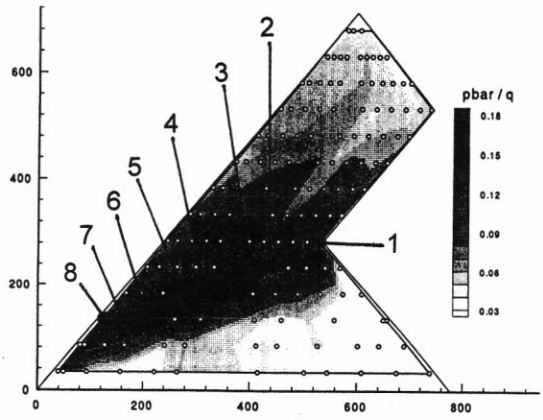

Figure 20a: Sample PSD Locations

PSD '1'

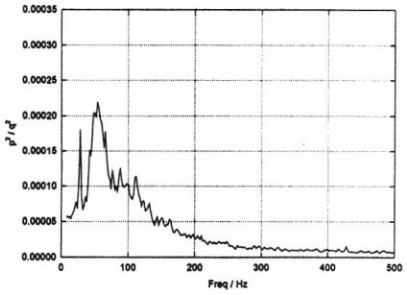

PSD '2'

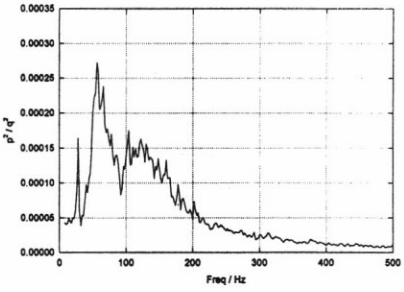

PSD '3'

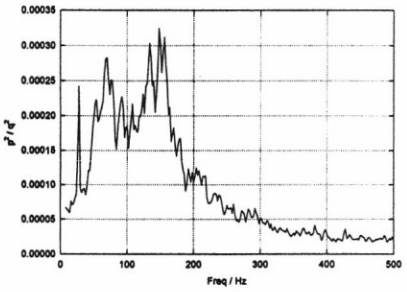

PSD '4'

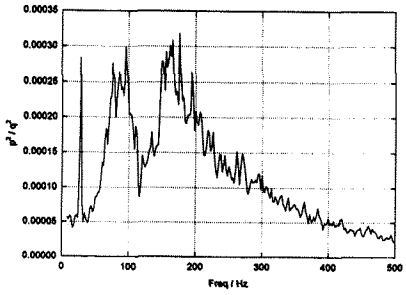

PSD '5'

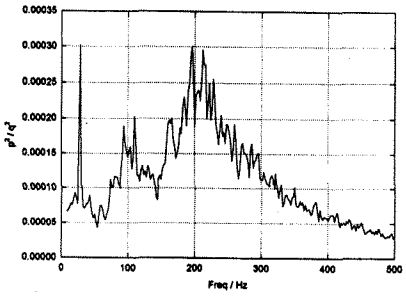

PSD '6'

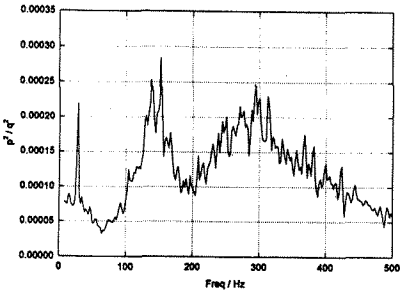

PSD '7'

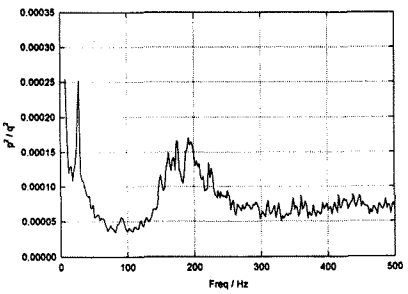

PSD '8'

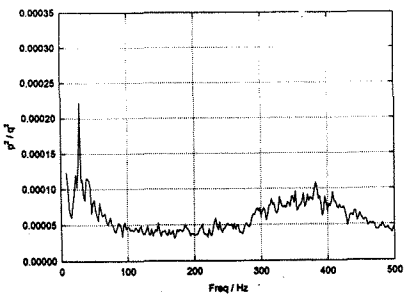

Figure 20b: PSDs Along Region of High RMS Pressure

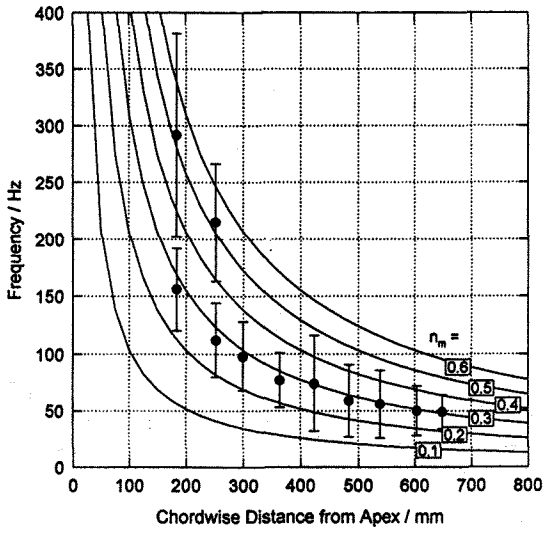

Figure 21: Variation of Centre Frequencies with Chordwise Location - Model 2, $\alpha = 14°$

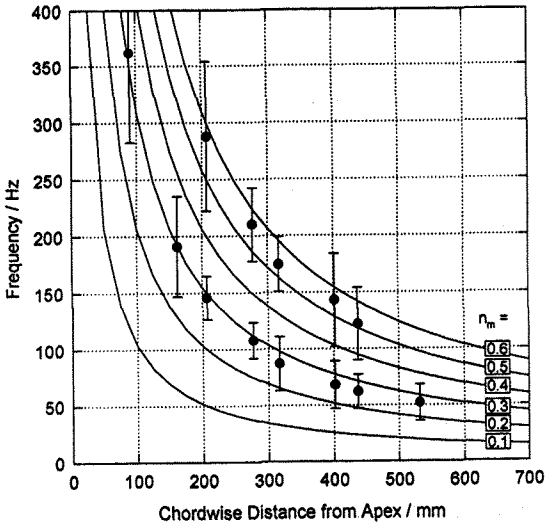

Figure 22: Variation of Centre Frequencies with Chordwise Location - Model 2, $\alpha = 14°$